Hindawi
International Journal of Antennas and Propagation
Volume 2023, Article ID 5171453, 15 pages
https://doi.org/10.1155/2023/5171453

Research Article

Identification of Control Parameters Using Taguchi Method for Hybrid Real-Binary Differential Evolution Algorithm and Its Applications in Electromagnetic Optimization

Wenchao Du,[1] Jianhui Wang,[1] Ruidong Wang,[2] Xingning Jia,[1] Guoche Qin,[1] and Chunshu Li[1]

[1]*School of Electronic and Electrical Engineering, Ningxia University, Yinchuan, Ningxia 750021, China*
[2]*School of Electrical Information Engineering, North Minzu University, Yinchuan, Ningxia 750030, China*

Correspondence should be addressed to Xingning Jia; nxujiaxn@nxu.edu.cn

Received 29 May 2023; Revised 15 November 2023; Accepted 12 December 2023; Published 22 December 2023

Academic Editor: Truong Khang Nguyen

The hybrid real-binary differential evolution (HDE) algorithm has been proficient in addressing electromagnetic optimization problems (EOPs) involving both real and binary variables. However, its optimization performance on different control parameter (CP) settings is not further studied, and the method to determine the values of CPs is more likely to use the trial-and-error method, which lacks universality on both unimodal and multimodal benchmarks. To completely account for the effect of CPs in HDE, the Taguchi method is utilized to identify the values of each CP. The orthogonal experiment result is the average rank of the mean values of 23 benchmark functions obtained by HDE and other classic optimization algorithms. Based on the analysis of variance results, three CPs that have a major effect on the performance of HDE are selected, and each of them is changed from level 1 to level 5 to further obtain the best combination of CPs, which is indicated as HDE_{N1}. To further enhance the local search ability of HDE_{N1} for the global best, a modified algorithm (HDE_{N2}) is proposed based on a novel mutation strategy selection method, and the simulation results demonstrate that the minimum values obtained by HDE_{N2} are smaller than those obtained by HDE_{N1}. Two EOPs, including planar microwave absorber and Yagi-Uda antenna designs, are solved to validate the performance of HDE_{N1} and HDE_{N2}. The results reveal that the HDE_{N1} and HDE_{N2} outperform HDE, demonstrating the efficacy of the proposed method for identifying the CPs of HDE. In the end, a low profile and wideband RCS reduction pixelated checkboard metasurface is optimized utilizing the HDE_{N2}, proving that the proposed algorithm can be a good candidate for hybrid real-binary electromagnetic problems.

1. Introduction

Many hybrid evolution algorithms have been proposed to address problems involving both real and binary parameters [1–6], and some of them have been utilized to solve antenna optimization problems such as antenna array synthesis [4, 5], material selection of microwave absorbers [6], and pixelated antenna design [4, 5]. A hybrid real-binary differential evolution (HDE) algorithm was proposed for antenna design in [5]. The optimization results of HDE were compared with those of hybrid real-binary particle swarm optimization (HPSO) [4], and the results demonstrated that HDE outperforms HPSO. The procedure for setting the control parameters (CPs) of HDE, however, was not explained.

As we know, despite the improved method for enhancing the performance of evolution algorithms, the control parameters (CPs) of each algorithm have greatly affected its optimization performance. As a result, it is critical to obtain the proper value of each CP. The traditional method usually adjusts the value of each CP via the trial-and-error method or empirical rules, resulting in an algorithm that is unsystematic and insufficiently generic for practical applications [7].

To address the issue of optimal CP setting, the Taguchi method (TM) was used for the identification of the strategy parameters of particle swarm optimization (PSO) [8, 9]. Four CPs, inertia weight ω, cognitive acceleration c_1, social acceleration c_2, and the maximum velocity along any dimension $V_{\max}$, were determined using TM in [8]. However, the result of each experiment was the mean fitness value of the best particle found for 50 independent runs of the Rosenbrock function, which was a multimodal benchmark function. The best combination of these four CPs was determined using the response table, and the performance of PSO with the new CPs was validated by the Griewank function. The simulation results revealed that better results were achieved by the PSO with the optimal CPs obtained through TM. The study in [9] investigated more than seven control factors of PSO based on the Taguchi method, and the experimental results for four benchmarks demonstrated that the population topology is the major factor in influencing PSO performance. The intrinsic limitation of this method is that it only considers two or four multimodal functions and lacks universality for other problems. Taguchi method was also adopted for finding the best combination of CPs for the ant colony optimization (ACO) algorithm [10]. The optimum combination of CPs of the ACO was determined by a response table, and the confirmation experiment was conducted to test the efficiency of the ACO with these CPs for a distribution allocation problem. However, from the perspective of optimization using the Taguchi method, the result of a confirmation experiment is not always better than the results of experiments established from the orthogonal array [11].

This paper proposes a new TM for CP selection of HDE by evaluating more than 23 benchmark functions. Six parameters, including different mutation operations, the number of populations, the upper and lower boundaries of the scaling factor, and the crossover rate for real and binary parts, respectively, are considered as the factors in the orthogonal experiment design. The main contributions of this paper are summarized as follows:

(1) To fully compare the performance of HDE on multimodal and unimodal functions, the result of each experiment in the Taguchi method is the average rank value, which is calculated among the mean values of 23 benchmark functions obtained by HDE with the CPs given in this experiment and other classic nature-inspired algorithms. To determine the best combination of CPs for HDE, the percent contributions of each factor are calculated, and the single factorial designs of the significant factors are evaluated. The ideal set of CPs for HDE is designated as HDE_{N1}.

(2) To enhance the ability to search the global optimum, a novel mutation strategy selection method is proposed to HDE_{N1}, which is denoted as HDE_{N2}. The simulation results show that the minimum values achieved by HDE_{N2} are less than those obtained by HDE_{N1} with a little sacrifice in convergence ability.

(3) The performance of HDE_{N1}, HDE_{N2}, and the original HDE is compared within three cases: benchmark functions and two electromagnetic optimization designs. Both the results of these cases show improved optimization performance and investigate the effectiveness of this method to select the proper CPs for HDE.

(4) A pixelated checkboard metasurface, which is on the lossy substrate backed by a 1-mm-thick aluminum plate with an air gap, is designed and has a lower profile and broader band of RCS reduction compared with the reference one.

2. Parameters Selection Using TM for HDE

2.1. The Control Parameters of HDE Algorithm. As depicted in [5], HDE combines classical DE and Boolean DE for real and binary parts, respectively. An individual of the population at generation G in HDE, denoted as $1 \le \mathrm{i} \le N_p$, where N_p is population size in the HDE, is also a candidate solution. For a hybrid real-binary minimization problem $F(\overrightarrow{X}_{i,G})$, where $\overrightarrow{X}_{i,G} = (\overrightarrow{X}^r_{i,G}, \overrightarrow{X}^b_{i,G})$ is a vector of $M + N$ dimensions, $\overrightarrow{X}^r_{i,G} = (R^1_{i,G}, R^2_{i,G}, \ldots, R^M_{i,G})$ and $\overrightarrow{X}^b_{i,G} = (B^1_{i,G}, B^2_{i,G}, \ldots, B^N_{i,G})$ represent real and binary variables, respectively.

Figure 1 shows the three main procedures of mutation, crossover, and selection. Different from the original HDE, there are six control parameters, such as mutation strategy (MS), population size N_p, the upper and lower boundaries of scaling factors $F_{\max}$ and $F_{\min}$ for real part as well as the crossover probabilities for real variables CR_r, and binary variables CR_b, respectively. Table 1 lists five mutation strategies for the real and binary parts of HDE. For real part, $\overrightarrow{V}^r_{i,G}$ denotes a mutated vector, and r_1, r_2, r_3, r_4, and r_5 are randomly chosen indices in the range $[1, \mathrm{Np}]$ such that $r_1 \ne r_2 \ne r_3 \ne r_4 \ne r_5 \ne i \in [1, \mathrm{Np}]$. $\overrightarrow{F}^r$ is a vector with M dimensions that the element is randomly chosen in the range $[F_{\min}, F_{\max}]$. It can be observed that the mutation strategies for binary parts convert the numeric operators "−," "+," and "−" in the mutation strategies for real parts into the logic operators "AND," "OR," and "XOR" accordingly. $r_n, n \in [1, 2, \ldots, 5]$ in binary part are same with the definition in the real part that $r_1 \ne r_2 \ne r_3 \ne r_4 \ne r_5 \ne j \in [1, \mathrm{Np}]$, and $\overrightarrow{F}^b$ is a random N-bit binary string. The binominal crossover operation is used independently to generate trial vectors $\overrightarrow{U}^r_{i,G}$ and $\overrightarrow{U}^b_{i,G}$ for real and binary parts, respectively. j_{rand} and k_{rand} are two randomly chosen integers in the ranges $[1, M]$ and $[1, N]$, respectively. randi is a uniform random number within the range [0, 1].

2.2. Parameters Selection Using TM. This section describes the detailed procedures for choosing the optimal CPs using TM for HDE with better performance. TM is a robust design approach based on the orthogonal array (OA) and signal-to-noise ratio (SNR) to study a large number of parameters with a limited number of experiments. OA, which is represented

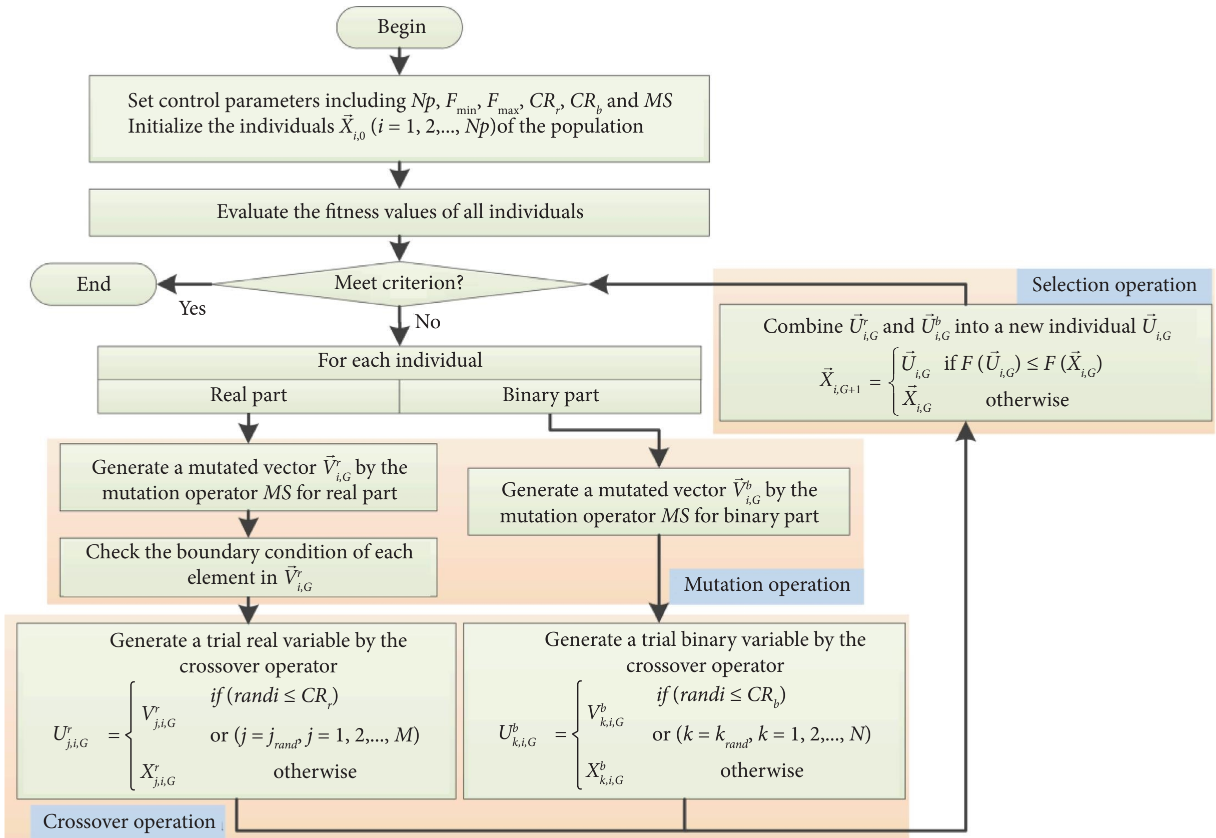

Figure 1: The flowchart of HDE.

by the notation $\mathrm{OA}(N_0, k, s, t)$, is utilized to design the experiments. Compared to the full factorial design, experiment design using OA may effectively reduce the number of experiments while maintaining the essential information. N_0 and k indicate the number of experiments to be conducted and the number of variables whose effects are about to be analyzed, respectively. s indicates the levels of each variable, and t suggests the strength. SNR, which is used to select the current best level of each variable, indicates the adaptation of the design parameters.

In this paper, OA (25, 6, 5, 2) is employed, and the factors with their corresponding level values are listed in Table 2. 23 functions, comprising 7 unimodal and 16 multimodal benchmark functions, are tested to further evaluate the performance of HDE on various types of benchmark functions. The detailed expression, including the upper and lower bounds of each function, can be found in [12]. All functions are tested on the assumption that partial real variables are represented by a binary string with a quantization error of less than 2×10^{-4}, as suggested in [6].

The result of each experiment is a mean rank value, which can be calculated as follows: first, the mean values of 23 benchmark functions with 100 independent runs are obtained by HPSO [4], IHPSO [6], GA, HGWO [13], BEO [14], and HDE_n, where HDE_n denotes the HDE algorithm with the combination of CPs in the n th experiment and $1 \le n \le N_0$. Second, the rank of the mean value of the m th benchmark function obtained by the HDE_n algorithm, denoted as r_{mn}, is calculated. Third, the average rank values of HDE_n by $\sum_{m=1}^{23} r_{mn}$ are calculated. Table 3 displays the factor values and results of each experiment, and the values of MS are shown as the level value. It is clear that the minimum result is obtained by the 25th experiment.

After all experiments are conducted, a response table based on (1) is created and displayed in Table 4.

$$\eta_{p,l} = -10 \lg \left(\frac{1}{m} \sum_{i=1}^{m} \left(f_i^{p,l} \right)^2 \right), \tag{1}$$

where $f_i^{p,l}$ denotes the i th experiment value of factor p at level l. m is the number of experiments in which the level of factor p is l. For a minimum problem, if all experiment results are greater than zero, "the larger the better" characteristic is selected for choosing the best level of each factor from the response table. Hence, the best level values for these six factors are 50, 0.2, 0.7, 0.9, 0.1, and 1 with respect to the levels (5, 2, 2, 5, 1, and 1), and the minimum SNRs of each factor are shown in bold. The average rank value for HDE with current CPs is 3, which is slightly larger than the result of the 25th experiment in Table 3. Additionally, from the analysis of variance (ANOVA) [15], the percent contribution of each factor is calculated, and the results show that the factors CR_b, MS, and N_p have a greater impact on the performance of HDE.

Table 1: Mutation strategy expressions in HDE.

Mutation strategy	Real part	Binary part
DE/rand/1	$\overrightarrow{V}^{r}_{i,G} = \overrightarrow{X}^{r}_{r1,G} + \overrightarrow{F}^{r} \cdot (\overrightarrow{X}^{r}_{r2,G} - \overrightarrow{X}^{r}_{r3,G})$	$\overrightarrow{V}^{b}_{j,G} = \overrightarrow{X}^{b}_{r1,G}$ OR $\overrightarrow{F}^{b}$ AND $(\overrightarrow{X}^{b}_{r2,G}$ XOR $\overrightarrow{X}^{b}_{r3,G})$
DE/rand/2	$\overrightarrow{V}^{r}_{i,G} = \overrightarrow{X}^{r}_{r1,G} + \overrightarrow{F}^{r} \cdot (\overrightarrow{X}^{r}_{r2,G} - \overrightarrow{X}^{r}_{r3,G}) + \overrightarrow{F}^{r} \cdot (\overrightarrow{X}^{r}_{r4,G} - \overrightarrow{X}^{r}_{r5,G})$	$\overrightarrow{V}^{b}_{j,G} = \overrightarrow{X}^{b}_{r1,G}$ OR $\overrightarrow{F}^{b}$ AND $(\overrightarrow{X}^{b}_{r2,G}$ XOR $\overrightarrow{X}^{b}_{r3,G})$ OR $\overrightarrow{F}^{b}$ AND $(\overrightarrow{X}^{b}_{r4,G}$ XOR $\overrightarrow{X}^{b}_{r5,G})$
DE/best/1	$\overrightarrow{V}^{r}_{i,G} = \overrightarrow{X}^{r}_{\text{best},G} + \overrightarrow{F}^{r} \cdot (\overrightarrow{X}^{r}_{r1,G} - \overrightarrow{X}^{r}_{r2,G})$	$\overrightarrow{V}^{b}_{i,G} = \overrightarrow{X}^{b}_{\text{best},G}$ OR $\overrightarrow{F}^{b}$ AND $(\overrightarrow{X}^{b}_{r1,G}$ XOR $\overrightarrow{X}^{b}_{r2,G})$
DE/best/2	$\overrightarrow{V}^{r}_{i,G} = \overrightarrow{X}^{r}_{\text{best},G} + \overrightarrow{F}^{r} \cdot (\overrightarrow{X}^{r}_{r1,G} - \overrightarrow{X}^{r}_{r2,G}) + \overrightarrow{F}^{r} \cdot (\overrightarrow{X}^{r}_{r3,G} - \overrightarrow{X}^{r}_{r4,G})$	$\overrightarrow{V}^{b}_{i,G} = \overrightarrow{X}^{b}_{\text{best},G}$ OR $\overrightarrow{F}^{b}$ AND $(\overrightarrow{X}^{b}_{r1,G}$ XOR $\overrightarrow{X}^{b}_{r2,G})$ OR $\overrightarrow{F}^{b}_{j}$ AND $(\overrightarrow{X}^{b}_{r3,G}$ XOR $\overrightarrow{X}^{b}_{r4,G})$
DE/current-to-best/1	$\overrightarrow{V}^{r}_{i,G} = \overrightarrow{X}^{r}_{i,G} + \overrightarrow{F}^{r} \cdot (\overrightarrow{X}^{r}_{\text{best},G} - \overrightarrow{X}^{r}_{i,G}) + \overrightarrow{F}^{r} \cdot (\overrightarrow{X}^{r}_{r1,G} - \overrightarrow{X}^{r}_{r2,G})$	$\overrightarrow{V}^{b}_{j,G} = \overrightarrow{X}^{b}_{j,G}$ OR $\overrightarrow{F}^{b}$ AND $(\overrightarrow{X}^{b}_{\text{best},G}$ XOR $\overrightarrow{X}^{b}_{j,G})$ OR $\overrightarrow{F}^{b}$ AND $(\overrightarrow{X}^{b}_{r1,G}$ XOR $\overrightarrow{X}^{b}_{r2,G})$

Table 2: Factors and the value of each level of the factor.

Level	Factors					
	N_p	$F_{\min}$	$F_{\max}$	CR_r	CR_b	MS
1	10	0.1	0.6	0.1	0.1	DE/rand/1
2	20	0.2	0.7	0.3	0.3	DE/rand/2
3	30	0.3	0.8	0.5	0.5	DE/best/1
4	40	0.4	0.9	0.7	0.7	DE/best/2
5	50	0.5	1	0.9	0.9	DE/current-to-best/1

Table 3: CPs and results of each experiment.

N_0	N_p	$F_{\min}$	$F_{\max}$	CR_r	CR_b	MS	Results
1	10	0.1	0.6	0.1	0.1	1	3.91
2	10	0.2	0.7	0.5	0.7	5	5.83
3	10	0.3	0.8	0.7	0.9	2	5.91
4	10	0.4	0.9	0.9	0.3	3	5.48
5	10	0.5	1	0.3	0.5	4	5.91
6	20	0.1	0.7	0.3	0.3	2	2.96
7	20	0.2	0.8	0.9	0.1	4	3.43
8	20	0.3	1	0.1	0.7	3	5.78
9	20	0.4	0.6	0.7	0.5	5	5.43
10	20	0.5	0.9	0.5	0.9	1	5.13
11	30	0.1	0.8	0.5	0.5	3	5.22
12	30	0.2	1	0.7	0.3	1	3.13
13	30	0.3	0.9	0.3	0.1	5	4.74
14	30	0.4	0.7	0.1	0.9	4	5.78
15	30	0.5	0.6	0.9	0.7	2	4.48
16	40	0.1	0.9	0.7	0.7	4	5.48
17	40	0.2	0.6	0.3	0.9	3	5.74
18	40	0.3	0.7	0.9	0.5	1	3.13
19	40	0.4	1	0.5	0.1	2	4.17
20	40	0.5	0.8	0.1	0.3	5	4.96
21	50	0.1	1	0.9	0.9	5	5.43
22	50	0.2	0.9	0.1	0.5	2	3.30
23	50	0.3	0.6	0.5	0.3	4	3.83
24	50	0.4	0.8	0.3	0.7	1	2.87
25	50	0.5	0.7	0.7	0.1	3	**2.83**

The bold value represents the lowest value among the results.

To further evaluate the influence of CR_b, MS, and N_p on the performance of HDE, the level of one of them is changing from 1 to 5 gradually while keeping the other CPs the same with the optimal level values obtained by the response table. Thus, a total of 13 extra experiments are conducted, and the minimum average rank value of 2.304 is obtained, as shown in Table 5. The corresponding CPs are $N_p = 30$, $F_{\min} = 0.2$, $F_{\max} = 0.7$, $\mathrm{CR}_r = 0.9$, $\mathrm{CR}_b = 0.1$, and DE/rand/1 mutation strategy, and HDE with these CPs is denoted as HDE_{N1}.

Table 6 displays the statistics of 23 benchmark functions that are optimized by 8 different algorithms, whose values of control parameters are listed in Table 7, used in under 100 independent runs, and the minimum average values of each benchmark function are shown in bold. The Ar in the last row denotes the average rank of the mean value of each benchmark obtained by different algorithms. As for the mean values, the results obtained by IHPSO are the best because Ar is the smallest at 2.87. The Ar of HDE_{N1} is 2.957, which is slightly larger than 2.87 for IHPSO and less than 4.957 for HDE, indicating that the search ability of HDE has improved with the new set of CPs. The lower standard deviation values of F_1 to F_{23} with the exception of F_8 are obtained by HDE_{N1}, showing that HDE_{N1} is more stable than HDE. However, the minimum results achieved by HDE_{N1} are greater than those of HDE, especially for the benchmarks with high dimensions. Because the mutation strategy of HDE is based on DE/best/1, and the population evolution of HDE has more potential to search around the global best to reach the global optimum, the minimum values obtained by HDE are lower than HDE_N for benchmarks with high dimension. However, it is more likely to be trapped in the local optimum for HDE with the DE/best/1 mutation strategy. For multimodal benchmark functions with fixed dimensions of F_{14} to F_{23}, HDE_{N1} performs better on the benefits of small landmarks and the DE/rand/1 mutation strategy and, therefore, has greater potential to thoroughly explore the search space.

In order to overcome the shortage of HDE_{N1} for lacking local search ability to find the optimum values, it is necessary to combine the DE/best/1 mutation strategy into the HDE_{N1} to increase its search ability around the global best. To enhance its local search ability of HDE_{N1}, a modified algorithm, which is denoted as HDE_{N2}, is proposed, and the details of HDE_{N2} are presented in Algorithm 1. After the first iteration of HDE, the population is sorted and divided into two parts depending on the fitness values. The subpopulation $S1$ consists of the Np/3 individuals with the best fitness values, and the remaining individuals form the subpopulation $S2$. At the mutation procedure, if the target vector is a member of subpopulation $S1$, the DE/best/1 is performed to generate the corresponding mutant vector; otherwise, the DE/rand/1 is used.

Table 6 shows the statistics of HDE_{N2} for benchmarks. From the perspectives of HDE and its two modified algorithms, the average results generated by HDE_{N1} and HDE_{N2} are better than those obtained by HDE, but the minimum values achieved by HDE_{N2} are less than those of HDE_{N1} and even close to the results of HDE. Although the Ar of HDE_{N2} is slightly greater than that of HDE_{N1}, the overall performance of HDE_{N2} is better than HDE.

To further compare the performance of these three algorithms, the stop criterion is set to the global optimum reaching f_c or the number of fitness function evaluations (NFFES) reaching 2×10^4. The statistics of success rates and running times of 23 benchmarks performed by HDE, HDE_{N1}, and HDE_{N2} are listed in Table 8. The success rate is the ratio of the number of runs that the global optimum reaches to f_c to 100 independent runs, and the times that have been consumed by 100 runs are also shown in Table 8. Actually, the running times of 13 benchmarks of HDE_{N2} are shorter than those of the other two algorithms. The success rates obtained by HDE_{N2} have increased by 10%–50% over those of HDE.

3. Applications in Electromagnetic Optimization

Three EOPs, PMA, Yagi-Uda antenna, and pixelated metasurface designs, are optimized in this section to validate the performance of HDE_{N2}.

Table 4: Response table.

Levels	Factors					
	N_p	$F_{\min}$	$F_{\max}$	CR_r	CR_b	MS
1	−14.748	−13.457	−13.521	−13.717	**−11.760**	**−11.428**
2	−13.418	**−12.984**	**−12.737**	−13.318	−12.443	−12.653
3	−13.540	−13.629	−13.295	−13.786	−13.520	−14.203
4	−13.607	−13.753	−13.792	−13.514	−14.003	−13.974
5	**−11.542**	−13.575	−13.985	**−13.062**	−14.975	−14.473
Optimal level values	50	0.2	0.7	0.9	0.1	1
Percent contribution	0.259	0.021	0.066	0.024	0.327	0.302

The bold values represent the lowest values of each column.

Table 5: Experiment results of HDE with fixed $F_{\min}$, $F_{\max}$, and CR_r and varying N_p, CR_b, and MS.

Factors	Experiments												
	1	2	3	4	5	6	7	8	9	10	11	12	13
N_p	10	20	30	40					50				
$F_{\min}$							0.2						
$F_{\max}$							0.7						
CR_r							0.9						
CR_b			0.1			0.3	0.5	0.7	0.9		0.1		
MS					1					2	3	4	5
Results	4.348	2.739	**2.304**	2.739	3.043	3.087	3.043	3.478	4.609	3.826	3.783	2.826	4.609

3.1. PMA Design. PMA design is a hybrid real-binary optimization problem in which the material and thickness are represented by a fixed-length binary string and a real number, respectively. The optimization goal is selecting the material with the appropriate thickness for each layer to minimize the reflection coefficient of an incident wave within the desired frequency band. In this section, a five-layered PMA design with PEC-backed is investigated, and its geometry is depicted in Figure 2. The detailed material parameters used in this case can be found in [16]. The incidence angle is denoted as θ, and the maximum thickness of each layer is 2 mm. The fitness function is defined as follows:

$$\text{Minimize}\, F(f,\theta) = R(f,\theta) + \gamma \max\left[0, \sum_{i=1}^{t} t_i - T_d\right], \quad (2)$$

where $R(f,\theta)$ represents the maximum reflection coefficient in decibels within the desired frequency band. The second term is a plenty function, which enables the overall thickness of PMA satisfy the design requirement. $\sum_{i=1}^{t} t_i$ denotes the actual overall thickness of PMA in the optimization process, and the maximum thickness of the PMA is represented by T_d, which is preset before the optimization. γ is set to 10^3, which is a larger number to ensure that the overall thickness of the final global best PMA design is smaller than T_d.

Two cases, denoted as case 1 and case 2, are optimized using five algorithms, namely, HDE [5], HPSO [4], IHPSO [6], HDE_{N1}, and HDE_{N2}, respectively. Cases 1 and 2 involve minimizing the reflection coefficient under normal incidence within the low-frequency band (0.2–2 GHz) and high-frequency band (2–8 GHz) with the constraint T_d = 5 mm. The statistics for the 20 independent runs are listed in Table 8, and Figure 3 shows the convergence curves. It is obvious that the average results obtained by HDE_{N2} are the lowest for both cases 1 and 2. The convergence curves versus the number of fitness function evaluations (NFFEs) obtained by HDE_{N1} and HDE at the early evolution show a significant difference in that HDE has a faster convergence speed than HDE_{N1} at the initial stage, due to the MS of HDE, i.e., DE/best/1, having more potential to search around the local optimum and get a better result. However, the hybrid MS selection method employed by HDE_{N2} can efficiently solve the lack of exploitation of HDE_{N1} and speed up the convergence at the early iterations. According to Table 9, the average and the minimum results obtained by HDE_{N2} are better than those obtained by HDE_{N1}. Furthermore, the minimum results optimized by HDE_{N2} are comparable to the minimum results obtained by HDE with only the DE/best/1 mutation strategy.

3.2. YAGI-UDA Antenna Design. In this section, a Yagi-Uda antenna is designed using HDE, HDE_{N1}, and HDE_{N2}, and the performance of the designs is compared. As shown in Figure 4, the traditional Yagi-Uda antenna consists of several linear dipole elements, one of which is energized directly by a feed transmission line. The total structure can be divided into three parts, including the driven element, reflector, and directors. The radiation performance of a Yagi-Uda antenna is comparable to that of an end-fire array since the parasitic elements in the front y-axis serve as directors and the rear dipole as a reflector. The currents of the reflector and directors are induced by mutual coupling [17]. In general, the lengths of the directors are slightly shorter than the driven element, while the length of the reflector is slightly longer. The Yagi-Uda in Figure 4 has a high gain along the x-axis, and the gain will be enhanced with the increasing number of directors. With the benefits of high

Table 6: Statistics of the different algorithm results of benchmark functions.

Functions	HPSO [4]		IHPSO [6]		GA		BEO [13]		HGWO [14]		HDE [5]			HDE_{N1}			HDE_{N2}		
	Ave	Std	Ave	Std	Ave	Std	Ave	Std	Ave	Std	Min	Ave	Std	Min	Ave	Std	Min	Ave	Std
F_1	8.03E−04	3.96E−03	**1.36E−05**	5.21E−05	1.35E−01	2.18E−01	7.02E+01	8.25E+01	2.37E+01	2.26E+02	3.64E−08	1.58E+01	3.36E+01	2.95E−04	1.11E−01	1.37E−01	4.44E−08	5.52E−02	2.11E−01
F_2	4.10E−03	3.10E−03	**6.45E−04**	4.20E−04	1.50E−01	6.46E−02	1.47E+00	8.02E−01	3.52E−03	3.77E−03	3.81E−04	3.25E−01	3.53E−01	1.06E−03	6.50E−02	6.30E−02	3.82E−04	5.27E−02	1.07E−01
F_3	1.89E+02	3.39E+02	**3.51E+01**	8.19E+01	3.25E+03	1.38E+03	2.81E+03	1.19E+03	4.03E+03	2.11E+03	0.03	9.13E+01	1.01E+02	22.14	1.40E+02	6.74E+01	7.15	1.11E+02	1.00E+02
F_4	1.06E+00	9.20E−01	**3.37E−01**	2.52E−01	5.63E+00	4.00E+00	1.83E+01	5.62E+00	4.29E+00	5.00E+00	2.49E−03	5.16E+00	4.52E+00	3.3	6.13E+00	1.94E+00	0.5	3.56E+00	1.54E+00
F_5	4.04E+02	5.77E+02	1.57E+02	3.71E+02	5.08E+02	6.66E+02	7.96E+03	1.51E+04	5.90E+03	4.65E+04	4.25	9.78E+02	2.11E+03	12.1	**4.15E+01**	4.52E+01	4.83	4.96E+01	6.80E+01
F_6	5.26E−01	2.54E−01	4.79E−01	2.41E−01	2.16E+00	6.14E−01	6.71E+01	7.01E+01	3.09E+01	2.91E+02	0.09	1.88E+01	4.17E+01	2.63E−02	**3.72E−01**	2.50E−01	8.61E−02	6.35E−01	9.17E−01
F_7	1.66E−02	1.08E−02	**1.43E−02**	8.39E−03	6.17E−02	3.88E−02	1.91E−01	1.25E−01	1.05E−01	2.46E−01	9.16E−03	4.70E−02	3.40E−02	1.40E−02	5.50E−02	1.90E−02	4.94E−03	4.83E−02	2.46E−02
F_8	−3.88E+03	3.39E+02	−4.53E+03	3.95E+02	−4.91E+03	2.67E+02	−4.98E+03	2.62E+02	**−5.48E+03**	2.26E+02	−5724.61	−4.96E+03	3.68E+02	−5794.94	−5.16E+03	4.35E+02	−5747.12	−5.14E+03	3.12E+02
F_9	2.30E+01	8.13E+00	2.02E+01	8.60E+00	2.24E+01	6.50E+00	2.76E+01	7.27E+00	**1.56E+01**	6.37E+00	7.21	3.18E+01	1.81E+01	7.32	5.36E+01	1.16E+01	4.53	3.76E+01	1.75E+01
F_{10}	6.09E−02	3.08E−01	**1.06E−02**	9.66E−02	2.19E+00	5.90E−01	3.77E+00	1.25E+00	1.97E+00	8.41E−01	1.31E−04	1.36E+00	1.19E+00	1.10E−02	3.12E−01	3.62E−01	1.47E−04	7.22E−01	7.80E−01
F_{11}	1.68E−01	1.19E−01	**6.75E−02**	5.74E−02	3.80E−01	1.57E−01	1.66E+00	8.64E−01	5.93E−01	1.96E+00	9.86E−03	5.79E−01	5.14E−01	0.21	5.89E−01	1.61E−01	4.50E−02	4.22E−01	2.23E−01
F_{12}	**9.62E−02**	7.49E−02	1.43E−01	1.71E−01	1.24E+00	1.02E+00	4.91E+00	2.26E+00	8.10E−01	7.40E−01	2.23E−03	4.82E−01	7.27E−01	1.44E−03	1.16E−01	3.65E−01	2.20E−03	4.96E−01	1.23E+00
F_{13}	2.64E−01	1.32E−01	**2.28E−01**	1.11E−01	1.01E+00	2.92E−01	5.24E+02	3.75E+03	6.96E+02	6.92E+03	0.21	2.01E+02	1.77E+03	6.34E−02	3.63E−01	5.87E−01	2.32E−02	3.69E−01	6.44E−01
F_{14}	2.75E+00	3.23E+00	2.14E+00	1.26E+00	7.90E+00	5.90E+00	**9.98E−01**	3.08E−05	3.23E+00	3.85E+00	0.998	2.27E+00	1.34E+00	0.998	1.08E+00	3.05E−01	0.998	1.30E+00	6.06E−01
F_{15}	3.01E−03	5.49E−03	2.46E−03	5.43E−03	9.39E−03	8.95E−03	1.29E−03	2.16E−03	1.69E−02	1.40E−02	5.86E−04	4.00E−03	7.00E−03	7.38E−04	**1.00E−03**	3.00E−04	5.91E−04	1.07E−03	1.96E−03
F_{16}	−1.03E+00	1.26E−02	−1.03E+00	7.86E−03	−1.01E+00	2.58E−02	−1.03E+00	3.16E−03	−9.96E−01	3.10E−02	−1.031	−1.03E+00	6.00E−03	−1.031	−1.03E+00	6.90E−06	−1.031	**−1.03E+00**	1.19E−04
F_{17}	4.12E−01	2.10E−02	4.04E−01	1.56E−02	4.43E−01	9.86E−02	3.99E−01	4.55E−03	6.19E−01	6.51E−01	0.399	3.99E−01	7.00E−03	0.398	**3.97E−01**	9.21E−06	0.398	3.98E−01	2.19E−05
F_{18}	3.00E+00	1.42E−06	3.00E+00	1.25E−06	1.15E+01	1.88E+01	3.00E+00	1.17E−06	2.26E+01	3.34E+01	3	3.81E+00	8.11E+00	3	3.00E+00	3.00E−03	3	**3.00E+00**	3.04E−06
F_{19}	−3.84E+00	3.64E−02	−3.86E+00	8.31E−03	−3.82E+00	8.80E−02	−3.86E+00	6.85E−04	−3.78E+00	1.53E−01	−3.86	−3.85E+00	3.08E−02	−3.86	−3.86E+00	5.00E−04	−3.86	**−3.86E+00**	2.62E−03
F_{20}	−3.23E+00	8.97E−02	−3.26E+00	6.52E−02	−3.19E+00	1.28E−01	−3.30E+00	3.16E−02	−3.13E+00	1.77E−01	−3.32	−3.27E+00	5.80E−02	−3.32	**−3.30E+00**	2.90E−02	−3.32	−3.29E+00	4.21E−02
F_{21}	−4.43E+00	2.90E+00	−5.44E+00	3.38E+00	−3.60E+00	2.68E+00	−6.04E+00	2.31E+00	−3.10E+00	2.44E+00	−10.153	−5.37E+00	3.00E+00	−10.153	**−7.77E+00**	2.13E+00	−10.152	−7.46E+00	2.49E+00
F_{22}	−5.00E+00	2.93E+00	−6.04E+00	3.36E+00	−3.21E+00	2.02E+00	−6.49E+00	2.51E+00	−2.54E+00	1.76E+00	−10.403	−6.23E+00	3.24E+00	−10.403	−8.45E+00	2.14E+00	−10.403	**−8.52E+00**	2.36E+00
F_{23}	−5.70E+00	3.36E+00	−6.66E+00	3.56E+00	−3.19E+00	1.88E+00	−6.76E+00	2.62E+00	−3.04E+00	2.28E+00	−10.536	−6.29E+00	3.46E+00	−10.536	−8.29E+00	2.44E+00	−10.536	**−8.98E+00**	2.12E+00
A_r	4.217		2.87		6.174		5.217		6.522			4.957			2.957			3.087	

The bold values are the lowest mean values of each function; it is necessary to show the lowest values in bold to probably evaluate the performance of each algorithm.

Table 7: Control parameters of each algorithm in Table 6.

Algorithms	Variable types	Control parameters
GA	Binary variables	Population size $N_p = 20$, crossover percentage Pc = 0.8, mutation percentage Pm = 0.3, mutation rate $\mu = 0.03$, roulette wheel selection, and selection pressure $\beta = 8$
BEO [13]		Population size $N_p = 20$, exploration ability control parameter $a_1 = 2$, exploitation ability control parameter $a_2 = 1$, and generation probability GP = 0.5
HGWO [14]		Population size $N_p = 20$, coefficient a is linearly decreased from 2 to 0 over the course of iterations, and inertia weight $w = 0.5 \times (1 + \text{rand})$
HPSO [4]	Hybrid variables	Population size $N_p = 20$, inertia weight for binary part $w_B = 1$, the upper and lower boundaries of inertia weights for real part $w_{R,\max} = 0.9$, $w_{R,\min} = 0.4$, accelerating coefficients $c_1 = c_2 = 2$, and the maximum velocities for real part and binary part, $\vec{V}_{R,\max} = 0.1 \times (\vec{R}_{\max} - \vec{R}_{\min})$, $V_{B,\max} = 6$
IHPSO [6]		All parameter sets are the same as the setting in HPSO
HDE [5]		Population size $N_p = 40$, the scaling factor $F = 0.7$, the crossover probabilities for real variables $CR_r = 0.8$, and binary variables $CR_b = 0.2$, mutation strategy: DE/best/1
HDE_{N1}		Population size $N_p = 30$, the upper and lower boundaries of scaling factors $F_{\max} = 0.7$ and $F_{\min} = 0.2$, the crossover probabilities for real variables $CR_r = 0.9$, and binary variables $CR_b = 0.1$, mutation strategy: DE/rand/1
HDE_{N2}		Population size $N_p = 30$, the upper and lower boundaries of scaling factors $F_{\max} = 0.7$ and $F_{\min} = 0.2$, the crossover probabilities for real variables $CR_r = 0.9$, and binary variables $CR_b = 0.1$, novel mutation strategy selection from DE/best/1 and DE/rand/1

```
Set Np = 30, F_min = 0.2, F_max = 0.7, CR_r = 0.9, CR_b = 0.1
Initialize the pop randomly distributed in the solution space.
Set gen = 0, FEs = 0, Max FEs = 10^4
while FEs ≤ MaxFEs do
      gen = gen + 1
   if gen > 1
      Sort the population based on their fitness values, and the top Np/3 individuals form subpopulation S1, and the remaining
   individuals form subpopulation S2.
   end if
for i = 1 ⟶ Np do
   if i ⊆ S1
      Perform the mutation operation based on DE/best/1.
   else
      Perform the mutation operation based on DE/rand/1.
   end
   Perform the crossover operation.
   Perform the selection operation.
end for
   FEs = FEs + Np
end while
Return the best agent fitness.
```

Algorithm 1: Pseudocode of HDE_{N2}.

gain, lightweight, simple configuration, and easy fabrication, Yagi-Uda antennas are primarily employed for TV and amateur radio applications.

In this scenario, FEKO, a 3D electromagnetic field solver based on the method of moments (MOM, the method of integral equation) [18, 19], is used to simulate a six-element Yagi-Uda antenna made up of a given length of dipoles. Table 10 displays the real-binary variables in relation to the electric parameters. The length of each linear dipole element $L_j\,(1 \le i \le 6)$ must be chosen from a set of lengths ranging from $0.3\lambda_0$ to $0.61\lambda_0$ with $0.01\lambda_0$ increment, where λ_0 is wavelength operating at 165 MHz in free space. As a result, each Yagi-Uda antenna element has 32 possible selections, and we need five bits to represent the choice length of each element. For example, the binary strings "00000" and "11111" represent the first and 32nd choices from the given length, i.e., $0.3\lambda_0$ and $0.61\lambda_0$. The spacing of each adjacent director $S_i\,(1 \le i \le 5)$ is a real variable that ranges from 0.01 to

Table 8: Statistics of success rates and running times of 23 benchmarks performed by HDE, HDE_{N1}, and HDE_{N2} at the criteria of either the global best reaching f_c or the NFFES reaching 2×10^4.

Functions	$f_{\min}$	f_c	Success rates HDE (%)	HDE_{N1} (%)	HDE_{N2} (%)	Times (s) HDE	HDE_{N1}	HDE_{N2}
F_1	0	$1.36E-05$	22	13	**58**	**1216.49**	1461.99	1297.74
F_1	0	$6.45E-04$	14	15	**58**	1482.24	1637.37	**1215.51**
F_3	0	35.1	71	86	**95**	**812.80**	950.44	817.99
F_4	0	0.337	**14**	2	**14**	1192.31	1257.03	**1123.93**
F_5	0	41.5	36	**95**	87	1070.54	692.13	**649.65**
F_6	0	0.372	21	**96**	66	1259.65	**783.79**	928.77
F_7	0	0.0143	**41**	6	19	1658.40	1657.20	**1519.22**
F_8	−5865.8	−5480	11	**52**	12	1140.49	**1063.66**	1175.29
F_9	0	15.6	73	31	**83**	**1116.22**	1620.31	1254.30
F_{10}	0	0.0106	24	**78**	42	1245.84	1200.16	**1042.69**
F_{11}	0	0.0675	16	31	**51**	1184.87	1156.77	**1048.72**
F_{12}	0	0.0962	51	**95**	70	844.21	**586.37**	772.00
F_{13}	0	0.228	2	**100**	96	1182.40	635.94	**552.72**
F_{14}	1	1	0	0	0	425.75	410.30	418.70
F_{15}	0.0003	0.001	48	**86**	**86**	485.74	319.04	**208.07**
F_{16}	−1.0316	−1.03	98	**100**	**100**	24.46	**22.14**	25.75
F_{17}	0.398	0.398	87	**100**	**100**	70.90	40.47	**28.25**
F_{18}	3	3	0	0	0	**447.35**	466.08	583.27
F_{19}	−3.86	−3.86	85	**100**	97	162.40	**48.94**	106.44
F_{20}	−3.32	−3.30	43	**90**	85	735.10	603.73	**506.76**
F_{21}	−10.1532	−7.77	28	**77**	66	602.29	442.56	**418.67**
F_{22}	−10.4028	−8.52	38	**75**	71	500.58	447.18	**413.41**
F_{23}	−10.5363	−8.98	31	**82**	**82**	617.20	439.38	**373.11**

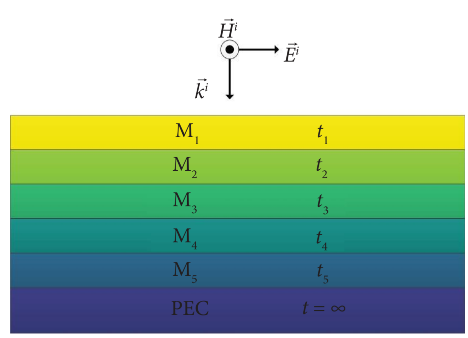

Figure 2: The configuration of PMA.

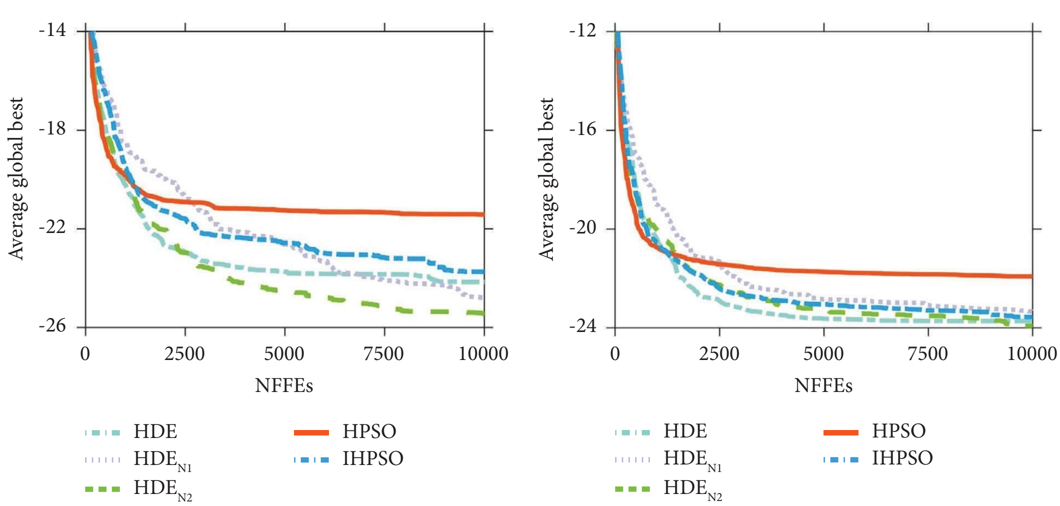

(a) (b)

Figure 3: The convergence curves of (a) case 1 and (b) case 2 optimized by HPSO, IHPSO, HDE, HDE_{N1}, and HDE_{N2}.

Table 9: The statistics of case 1 and case 2 for PMA designs.

Algorithms	Case 1 (0.2–2) GHz				Case 2 (2–8) GHz			
	Max	Min	Avr	Std	Max	Min	Avr	Std
HPSO [4]	−16.74	−28.38	−21.42	4.09	−17.5	−24.1	−21.92	1.77
IHPSO [6]	−17.18	−28.38	−23.74	4.93	−22.28	−25.34	−23.57	0.73
HDE [5]	−17.20	−28.38	−24.16	3.47	−20.94	−25.78	−23.73	1.06
HDE_{N1}	−16.99	−28.04	−24.80	2.70	−22.05	−25.35	−23.37	0.73
HDE_{N2}	−21.39	−28.37	−25.43	2.61	−22.36	−25.46	−23.92	0.86

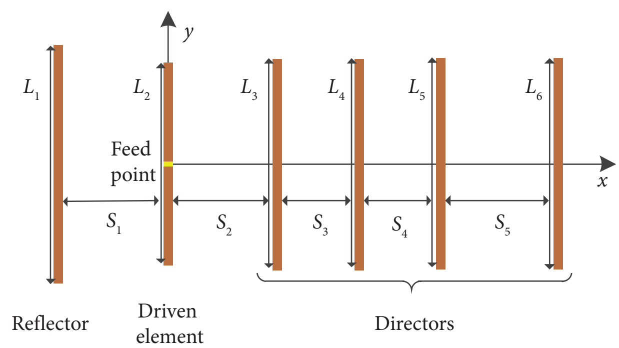

Figure 4: Six-element Yagi-Uda antenna configuration.

Table 10: The real and binary variables in HDE for Yagi-Uda antenna design.

	Real variable					Binary variable					
	S_1	S_2	S_3	S_4	S_5	L_1	L_2	L_3	L_4	L_5	L_6
	$S_i \in [0.01, 0.5]$, $(1 \le i \le 5)$					$L_j \in (00000 \sim 11111)$, $(1 \le j \le 6)$					
$\overrightarrow{X}_{i,G}$	0.217	0.199	0.364	0.408	0.37	10010	01111	01111	01101	01100	01100
Electric parameters	$0.217\lambda_0$	$0.199\lambda_0$	$0.364\lambda_0$	$0.408\lambda_0$	$0.37\lambda_0$	$(19)0.48\lambda_0$	$(16)0.45\lambda_0$	$(16)0.45\lambda_0$	$(14)0.43\lambda_0$	$(13)0.42\lambda_0$	$(13)0.42\lambda_0$

0.5 times λ_0. The total hybrid variables consist of five real variables and thirty bits of binary variables, like $\overrightarrow{X}_{i,G}$ in Table 9. The radius of each dipole is fixed to $0.003369\lambda_0$ in the physical model.

It is known from [17] that the best directivity of a six-element Yagi-Uda antenna is 13.41 dB without taking into account the front-to-back ratio (FBR). Therefore, the optimization objective is to reduce the FBR as much as possible while increasing the directivity over 13.41 dB. The fitness function can be expressed as follows:

$$\text{Minimize } F = \gamma \max\{0, 13.41 - D\} - \text{FBR}, \quad (3)$$

$$\text{FBR} = 20\log_{10}\left(\frac{E(\theta = 90^\circ, \phi = 0^\circ)}{\max\{E(\theta = 90^\circ, \phi_b)\}}\right), \quad (4)$$

where the first term in (3) is a plenty function to ensure that the directivity of a six-element Yagi-Uda antenna, which is denoted as D, is less than 13.41 dBi. FBR is calculated by (4), which denotes the ratio of the electric field at point $(\theta = 90^\circ, \phi = 0^\circ)$ to the maximum electric field at the points $(\theta = 90^\circ, \phi_b \in [160^\circ, 200^\circ])$. γ is set to 10^3 in this case to ensure that the directivity criterion is met first and next to make the FBR as larger as possible during the optimization.

The maximum NFFEs is 10^4 in this case, and each algorithm is run five times independently. Table 11 gives the obtained statistics and CP values of HDE, HDE_{N1}, and HDE_{N2} for Yagi-Uda antenna designs. The best average result is obtained by HDE_{N1}, and the design with the lowest fitness value is obtained by HDE_{N2}. The success rate in Table 10 denotes the ratio of the number of runs satisfied with the plenty term in (3) to five independent runs. HDE has a success rate of only 60%, showing that it is ineffective in this case. Figure 5(a) displays the average convergence curves obtained by HDE, HDE_{N1}, and HDE_{N2}. The minimum F value achieved by HDE_{N2} is −24.7, which is 3.1 less than the minimum F value obtained by HDE. From the directivity pattern shown in Figure 5(b), the lower front-back ratio is obtained by HDE_{N2}. The optimal result obtained by HDE_{N2} is $\{0.217\lambda_0, 0.199\lambda_0, 0.364\lambda_0, 0.408\lambda_0, 0.37\lambda_0, 1, 0, 0, 1, 0, 0, 1, 1, 1, 1, 0, 1, 1, 1, 1, 0, 1, 1, 0, 1, 0, 1, 1, 0, 0, 0, 1, 1, 0, 0\}$. Hence, the lengths of six dipoles are $L_1 = 0.48\lambda_0$, $L_2 = 0.45\lambda_0$, $L_3 = 0.45\lambda_0$, $L_4 = 0.43\lambda_0$, $L_5 = 0.42\lambda_0$, and $L_6 = 0.42\lambda_0$, respectively.

Table 11: The statistics for Yagi-Uda antenna designs.

Algorithms	Parameters setting	Max	Min	Avr	Success rate (%)
HDE [5]	$N_p = 40, F = 0.7, CR_r = 0.8, CR_b = 0.2$, DE/best/1	626.25	−21.60	158.15	60
HDE_{N1}	$N_p = 20, F_{min} = 0.2, F_{max} = 0.7, CR_r = 0.9, CR_b = 0.1$, DE/rand/1	−20.01	−23.94	−22.75	100
HDE_{N2}	$N_p = 30, F_{min} = 0.2, F_{max} = 0.7, CR_r = 0.9, CR_b = 0.1$, DE/rand/1, DE/best/1	−20.38	−24.7	−20.85	100

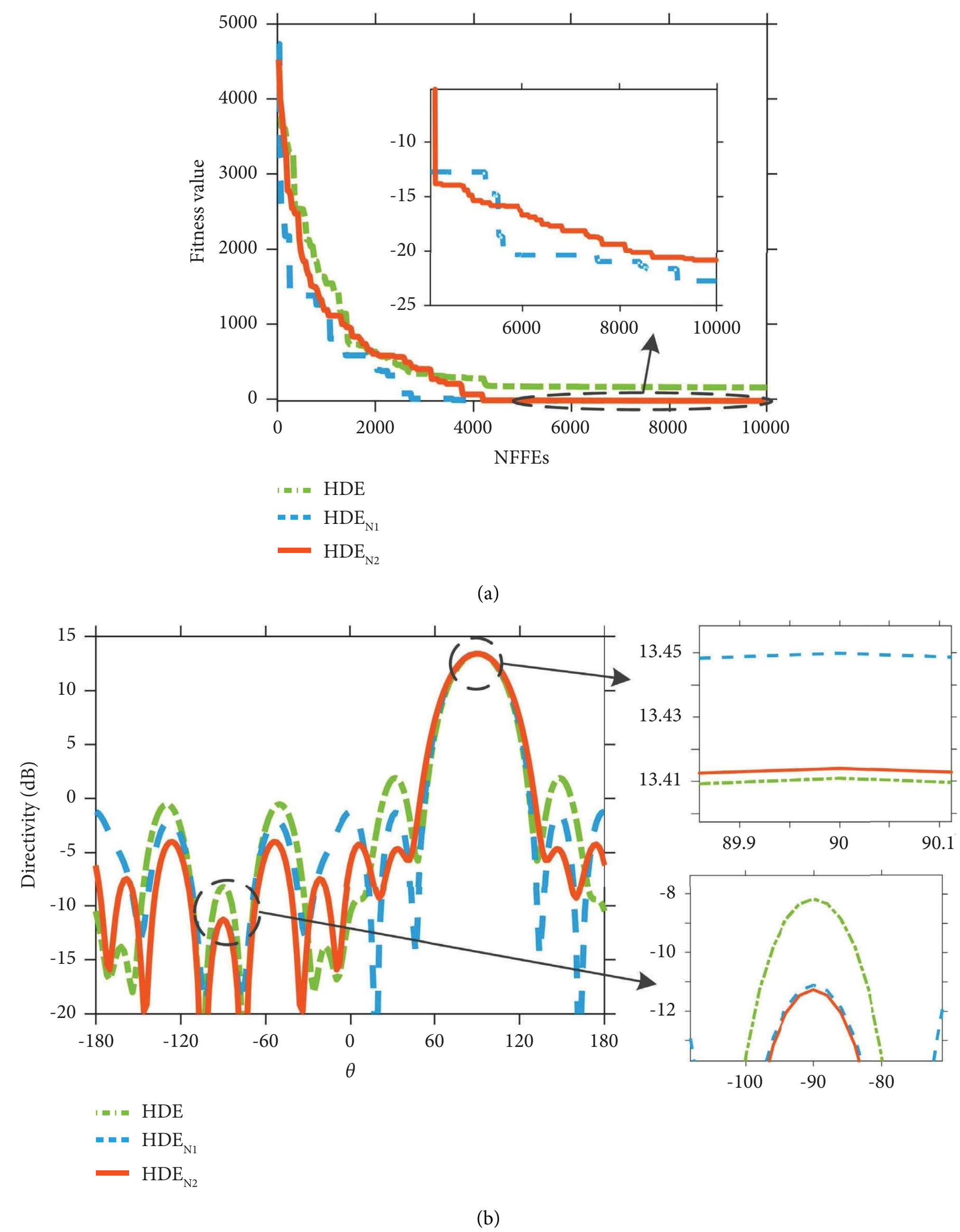

Figure 5: (a) Average convergence curves and (b) directivity versus θ of six-element Yagi-Uda antenna optimization using HDE, HDE_{N1}, and HDE_{N2}.

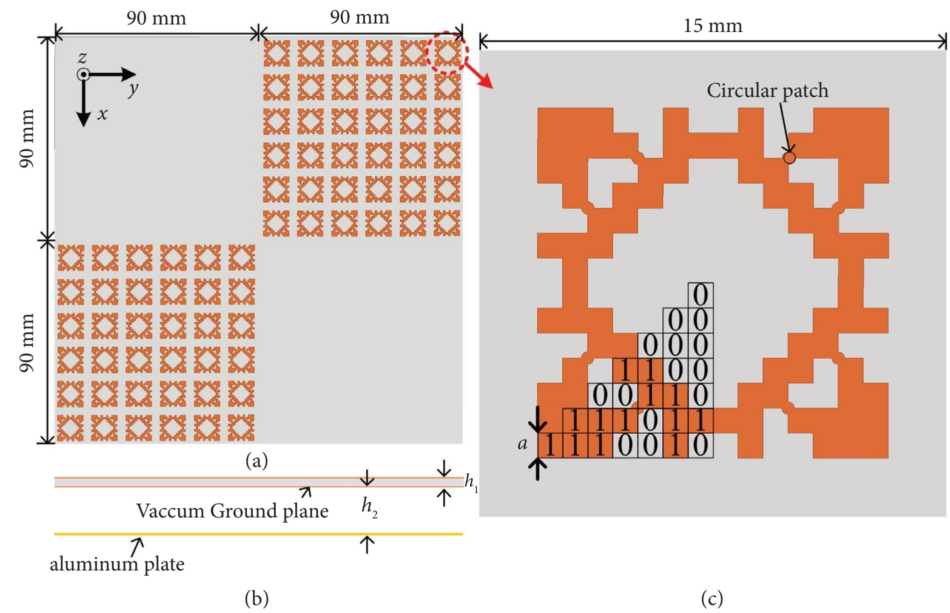

Figure 6: Configuration of the designed RCS reduction CM. (a) Top view, (b) side view, and (c) the layout of the pixelated unite cell.

3.3. Wideband RCS Reduction Checkerboard Metasurface Design. Checkerboard metasurface (CM) is one type of metasurface that has been widely used for radar cross section (RCS) reduction [20–22]. A pixelated CM is proposed in [21] over a frequency band from 3.8 to 10.7 GHz; however, the size of two cells is preassigned manually. A CM composed of pixelated and no-element tiles on a 1.57-mm-thick lossy FR-4 substrate ($\varepsilon_r = 4.4,\ \tan\sigma = 0.02$) backed by a 1-mm-thick aluminum plate with an h_2-thick air gap is designed, and the overall configuration is shown in Figure 6.

From Figure 6(c), the square patch is discretized into 14×14 pixels, and each pixel is represented by a square with a side length of a mm. To maintain the polarization independent, a four-fold symmetry is imposed into the patch, and then, the patch can be represented by a 28-bit binary string. Moreover, a circular patch with a radius of 0.2 mm is attached to a diagonal connection point to avoid one-point subpatch contacts. To realize the 10 dB RCS reduction over the frequency band from 4 to 12 GHz, the cell configuration represented by a vector consisting of a and h_2, and a 28-bits binary string is optimized using HDE_{N2}.

An approximated RCS reduction expression (5) in [23] is used as the fitness function in this case because of the reflection magnitude varying versus working frequency on a lossy substrate. The two real variables, which fluctuate in 0.1 mm steps, are optimized within $a \in [0.3, 1]$, $h_2 \in [0, 5]$.

$$R(f_i) = 10\log\left[\frac{A_1(f_i)e^{jP_1(f_i)} + A_2(f_i)e^{jP_2(f_i)}}{2}\right]^2, \quad (5)$$

where $A_1(f_i)$ and $P_1(f_i)$ denote the reflection amplitude and phase of the cell 1 at the ith operating frequency. The fitness function for the CM optimization is defined as follows:

$$\text{Minimize}, F = \frac{1}{n}\sum_{i=1}^{n} Q(f_i),$$
$$\text{s.t.,} \quad Q(f_i) = \begin{cases} -10, & R(f_i) \le -10, \\ R(f_i), & \text{otherwise}, \end{cases} \quad (6)$$

where f_i denotes the ith sampling frequencies within the given operating band 4–12 GHz. The stopping criterion is $F = -10$ or the maximum NFFE reaching to 2000.

The reflection coefficients of pixelated and no-element unite cells are carried out using the CST MICROWAVE STUDIO® [24]. The control parameters of HDE_{N2} are same with the setting of the design of the Yagi-Uda antenna. The optimal result which is represented by a vector of $\vec{x} = \{0.8, 4.4, 1, 1, 1, 0, 0, 1, 0, 1, 1, 1, 0, 1, 1, 0, 0, 1, 1, 0, 1, 1, 0, 0, 0, 0, 0, 0, 0, 0\}$ is obtained after 265 fitness function evaluations.

One period of a square CM that combines pixelated and no-element tiles is depicted in Figure 6(a). Each tile consists of 6×6 cells to mimic the periodic boundary condition. Figure 7 shows that 100% and almost 96% fractional bandwidths of monostatic 10 dB RCS reductions are obtained by the simulated and approximate results, respectively. The deviation occurs due to the lack of mutual coupling consideration of the predicted expression (5). The total thickness of our proposed metasurface is 5.97 mm, which is lower than case 3 of [22], and a wider RCS reduction band is obtained, as listed in Table 12.

The simulated 3D bistatic scattered fields at 4.5, 6.5, 8.5, and 11.5 GHz under the normal incidence of our proposed CM are depicted in Figure 8. It is clear that the energy is mainly redirected in the diagonal planes: $\phi = 45^\circ, 135^\circ, 225^\circ, 315^\circ$ and dramatically reduced along the xz and yz planes. The RCSs of the proposed metasurface and

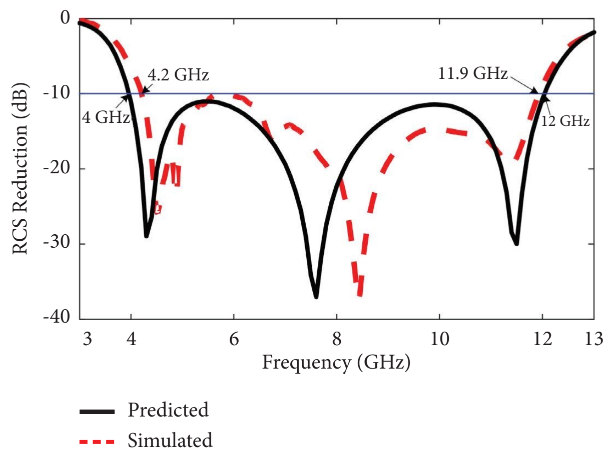

Figure 7: Simulated and predicted RCS reduction of the optimal CM.

Table 12: Comparisons of the simulated −10 dB RCS reduction band, fractional bandwidth, and total thickness of metasurface.

Ref	Simulated −10 dB RCS reduction band (GHz)	Fractional bandwidth (%)	Total thickness (mm)
Case 3/[22]	4.2–11.6	94	6.57
This work	4.2–11.9	96	5.97

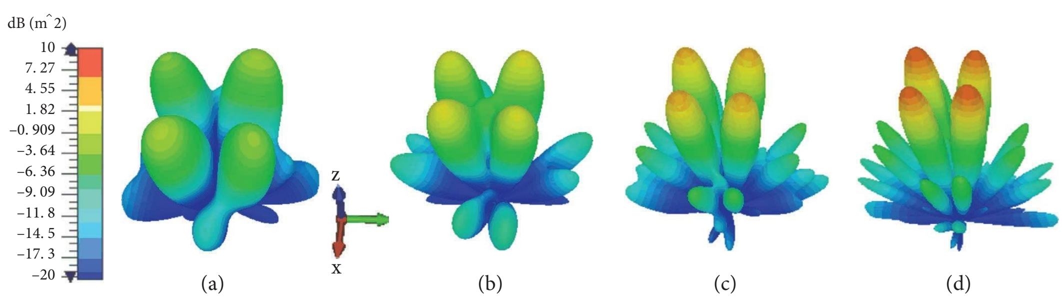

Figure 8: Simulated 3D bistatic scattered fields at (a) 4.5 GHz, (b) 6.5 GHz, (c) 8.5 GHz, and (d) 11.5 GHz of the optimal design.

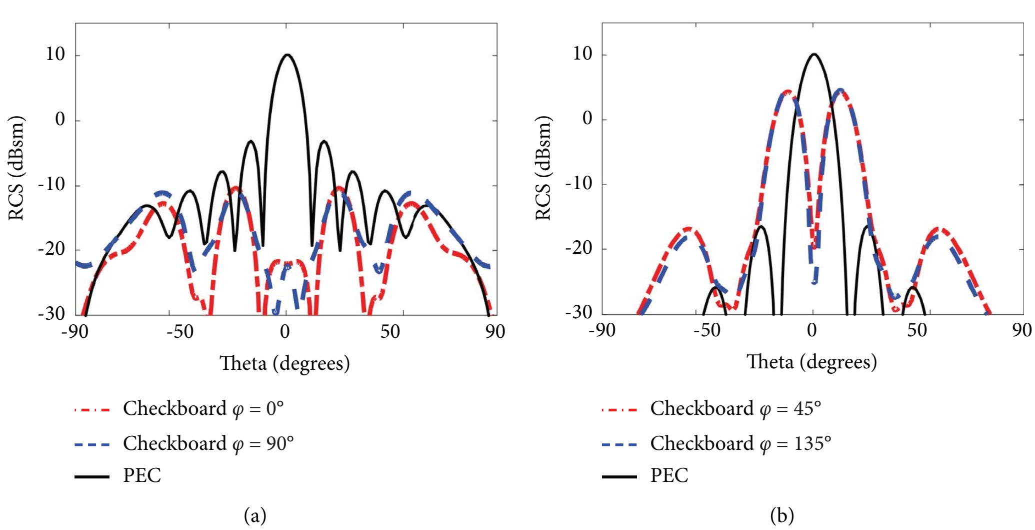

Figure 9: Simulated RCS of the proposed metasurface and equal-sized PEC plane at 8.5 GHz versus elevation angle θ at (a) $\phi = 0^\circ$ or 90° plane and (b) $\phi = 45^\circ$ or 135° planes.

equal-sized PEC plane versus θ at $\phi = 0^\circ, 45^\circ, 90^\circ, 135^\circ$ are shown in Figure 9 that the maximum RCS of the proposed metasurface at $\phi = 0^\circ$ or 90° plane is 20.5 dB lower than that of the PEC plane and 5.6 dB at $\phi = 45^\circ$ or 135° plane, respectively.

4. Conclusions

In this paper, the Taguchi method is used to determine the CPs of HDE by averaging the performance ranks of 23 benchmark functions for the universality of multimodal and unimodal problems. The overall performance of HDE with newly identified CPs, named HDE_{N1}, is superior to HDE by benchmark comparisons, which demonstrates the effectiveness of the proposed method. The contribution percentages of each CP are calculated, and the results reveal that crossover probability for the binary part, population size, and mutation strategy are three factors that have the most influence on HDE performance. The mutation strategy DE/rand/1 in HDE_{N1} improves the exploration ability of HDE but is short at the exploitation. As a result, a novel mutation strategy selection method is proposed to enhance its search performance, named HDE_{N2}. The results of two classic EOPs indicate that the HDE_{N2} has more power to handle real-binary EOPs. In addition, we employ HDE_{N2} to design a lower profile and wider RCS reduction bandwidth pixelated checkboard metasurface than the reference one. All results indicate that our proposed method for identifying the CPs of HDE and improving the search ability of HDE is successful.

Furthermore, this method can be used to identify the CPs of other algorithms as well. For the result of an experiment using the Taguchi method, not only the mean value but also the linear combination of the average rank values of minimum value, mean value, and standard deviation might be an acceptable alternative. Meanwhile, the analysis of variance can give the percent contribution of each CP, allowing us to propose new methods to the most relevant CPs in order to improve the optimization performance of the algorithm.

Data Availability

The data used to support the findings of this study are available from the corresponding author upon request.

Conflicts of Interest

The authors declare that they have no conflicts of interest.

Acknowledgments

This work was supported in part by the Natural Science Foundation of Ningxia Province under Grant 2022AAC03116, Grant 2021AAC03193, and Grant 2022AAC03051 and Key Research and Development Program of Ningxia Province under Grant 2021BEB04068.

References

[1] T. Liao, K. Socha, M. A. M. de Oca, T. Stützle, and M. Dorigo, "Ant colony optimization for mixed-variable optimization problems," *Institute of Electrical and Electronics Engineers Transactions on Evolutionary Computation*, vol. 18, no. 4, pp. 503–518, 2013.

[2] Y. Lin, Y. Liu, W. N. Chen, and J. Zhang, "A hybrid differential evolution algorithm for mixed-variable optimization problems," *Information Sciences*, vol. 466, pp. 170–188, 2018.

[3] H. Peng, Y. Han, C. Deng, J. Wang, and Z. Wu, "Multi-strategy co-evolutionary differential evolution for mixed-variable optimization," *Knowledge-Based Systems*, vol. 229, Article ID 107366, 2021.

[4] N. Jin and Y. Rahmat-Samii, "Hybrid real-binary particle swarm optimization (HPSO) in engineering electromagnetics," *Institute of Electrical and Electronics Engineers Transactions on Antennas and Propagation*, vol. 58, no. 12, pp. 3786–3794, 2010.

[5] L. Xie and Y. C. Jiao, "Hybrid real-binary differential evolution algorithm applied to antenna optimization," *Microwave and Optical Technology Letters*, vol. 54, no. 6, pp. 1460–1463, 2012.

[6] X. Jia, G. Qin, and C. Li, "Improved hybrid real-binary PSO using modified learning and restarting methods for planar microwave absorber designs," *Institute of Electrical and Electronics Engineers Access*, vol. 11, pp. 15505–15513, 2023.

[7] R. Gämperle, S. D. Müller, and P. Koumoutsakos, "A parameter study for differential evolution," *Advances in intelligent systems, fuzzy systems, evolutionary computation*, vol. 10, no. 10, pp. 293–298, 2002.

[8] A. Khosla, S. Kumar, and K. K. Aggarwal, "Identification of strategy parameters for particle swarm optimizer through Taguchi method," *Journal of Zhejiang University- Science*, vol. 7, no. 12, pp. 1989–1994, 2006.

[9] H. Wang, Q. Geng, and Z. Qiao, "Parameter tuning of particle swarm optimization by using Taguchi method and its application to motor design," in *Proceedings of the 2014 4th IEEE international conference on information science and technology*, pp. 722–726, Shenzhen, China, April 2014.

[10] V. Vinay and R. Sridharan, "Taguchi method for parameter design in ACO algorithm for distribution–allocation in a two-stage supply chain," *The International Journal of Advanced Manufacturing Technology*, vol. 64, no. 9-12, pp. 1333–1343, 2013.

[11] X. Jia and G. Lu, "An improved taguchi's method for electromagnetic applications," *Progress In Electromagnetics Research Letters*, vol. 87, pp. 89–96, 2019.

[12] S. Mirjalili and A. Lewis, "The whale optimization algorithm," *Advances in Engineering Software*, vol. 95, pp. 51–67, 2016.

[13] Q. Al-Tashi, S. J. Abdul Kadir, H. M. Rais, S. Mirjalili, and H. Alhussian, "Binary optimization using hybrid grey wolf optimization for feature selection," *Institute of Electrical and Electronics Engineers Access*, vol. 7, pp. 39496–39508, 2019.

[14] A. Faramarzi, S. Mirjalili, and M. Heidarinejad, "Binary equilibrium optimizer: theory and application in building optimal control problems," *Energy and Buildings*, vol. 277, Article ID 112503, 2022.

[15] T. Mori, *Taguchi Methods: Benefits, Impacts, Mathematics, Statistics, and Applications*, ASME Press, New York, NY, USA, 2011.

[16] E. Michielssen, J. M. Sajer, S. Ranjithan, and R. Mittra, "Design of lightweight, broad-band microwave absorbers using genetic algorithms," *Institute of Electrical and Electronics Engineers Transactions on Microwave Theory and Techniques*, vol. 41, no. 6, pp. 1024–1031, 1993.
[17] C. A. Balanis, *Antenna Theory: Analysis and Design*, John Wiley & Sons, Hoboken, NJ, USA, 2015.
[18] S. N. Makarov, V. Iyer, and S. Kulkarni, *Antenna and EM Modeling with MATLAB Antenna Toolbox*, John Wiley & Sons, Hoboken, NJ, USA, 2021.
[19] Feko, "Altair engineering inc," 2020, https://altair.com/feko.
[20] J. Su, Y. Lu, J. Liu, Y. Yang, Z. Li, and J. Song, "A novel checkerboard metasurface based on optimized multielement phase cancellation for superwideband RCS reduction," *Institute of Electrical and Electronics Engineers Transactions on Antennas and Propagation*, vol. 66, no. 12, pp. 7091–7099, 2018.
[21] M. J. Haji-Ahmadi, V. Nayyeri, M. Soleimani, and O. M. Ramahi, "Pixelated checkerboard metasurface for ultra-wideband radar cross section reduction," *Scientific Reports*, vol. 7, no. 1, Article ID 11437, 017.
[22] A. Murugesan, D. Natarajan, and K. T. Selvan, "Low-cost, wideband checkerboard metasurfaces for monostatic RCS reduction," *Institute of Electrical and Electronics Engineers Antennas and Wireless Propagation Letters*, vol. 20, no. 4, pp. 493–497, 2021.
[23] W. Chen, C. A. Balanis, and C. R. Birtcher, "Checkerboard EBG surfaces for wideband radar cross section reduction," *Institute of Electrical and Electronics Engineers Transactions on Antennas and Propagation*, vol. 63, no. 6, pp. 2636–2645, 2015.
[24] C. S. Suite, "Computer simulation technology ag," 2023, http://www.cst.com.